Geophysical Research Letters

RESEARCH LETTER
10.1029/2019GL083948

Turbulence and Gas Transfer Velocities in Sheltered Flooded Forests of the Amazon Basin

Sally MacIntyre[1,2], Joao H. Fernandes Amaral[1,3], Pedro M. Barbosa[1], Alicia Cortés[1], Bruce R. Forsberg[3], and John M. Melack[1,2]

[1]Earth Research Institute, University of California, Santa Barbara, CA, USA, [2]Department of Ecology, Evolution and Marine Biology, University of California, Santa Barbara, CA, USA, [3]Laboratório de Ecossistemas Aquáticos, Instituto Nacional de Pesquisas da Amazônia, Manaus, Brazil

Key Points:
- Gas transfer velocities in flooded forests ranged from 1 to 5 cm/hr
- Under cooling, convection dominates turbulence production
- Under heating, turbulence was suppressed unless influenced by wind-generated motions from the adjacent open water

Supporting Information:
- Supporting information S1

Correspondence to:
S. MacIntyre,
sally@eri.ucsb.edu

Citation:
MacIntyre, S., Amaral, J. H. F., Barbosa, P. M., Cortés, A., Forsberg, B. R., & Melack, J. M. (2019). Turbulence and gas transfer velocities in sheltered flooded forests of the Amazon Basin. *Geophysical Research Letters*, *46*, 9628–9636. https://doi.org/10.1029/2019GL083948

Received 31 MAY 2019
Accepted 5 AUG 2019
Accepted article online 7 AUG 2019
Published online 27 AUG 2019

Abstract Seasonally flooded forests along tropical rivers cover extensive areas, yet the processes driving air-water exchanges of radiatively active gases are uncertain. To quantify the controls on gas transfer velocities, we combined measurements of water-column temperature, meteorology in the forest and adjacent open water, turbulence with an acoustic Doppler velocimeter, gas concentrations, and fluxes with floating chambers. Under cooling, measured turbulence, quantified as the rate of dissipation of turbulent kinetic energy (ε), was similar to buoyancy flux computed from the surface energy budget, indicating convection dominated turbulence production. Under heating, turbulence was suppressed unless winds in the adjacent open water exceeded 1 m/s. Gas transfer velocities obtained from chamber measurements ranged from 1 to 5 cm/hr and were similar to or slightly less than predicted using a turbulence-based surface renewal model computed with measured ε and ε predicted from wind and cooling.

Plain Language Summary Flooded forests are widespread in the tropics and occur elsewhere. Within the lowland Amazon basin, seasonally inundated forests cover about 15% of the total area and are important to the ecology of the region. Concentrations of greenhouse gases can be high, indicating that flooded forests are likely an appreciable source of these gases to the atmosphere. To understand drivers of gas exchange, measurements of meteorology, temperature, and turbulence in the water were performed in Amazonian flooded forests. While air in flooded forests is often still, water immediately below is in motion and turbulent. The combination of wind-driven flows from outside the forest and nocturnal cooling within the forests indicates that near-surface turbulence is sustained in the flooded forest. Consequently, the extensive area of flooded forests will release appreciable amounts of greenhouse.

1. Introduction

Computing fluxes of radiatively active gases, such as CO_2 and CH_4, from the large regions with flooded forests in the tropics and elsewhere requires a mechanistic understanding of the drivers of gas transfer velocities within the forests. Turbulence associated with wind is known to drive exchange of gases across the air-water interface at exposed locations even with light winds (MacIntyre et al., 2010; Wang et al., 2015; Zappa et al., 2007). Controls on turbulence within sheltered flooded forests may differ. With little to no wind, the expectation is that turbulence and related gas transfer velocities would depend on negative buoyancy flux, that is, heat loss, for much of the time (MacIntyre et al., 2018; Schladow et al., 2002). Rather than depending on winds within forests, near-surface turbulence may depend on flows induced by adjacent open water (Augusto-Silva et al., 2018) and differential heating and cooling (Monismith et al., 1990).

Turbulence can be incorporated into computations of gas fluxes when the gas transfer velocity is based on the surface renewal model (SRM). Flux, $F = k\,(C_w - C_{eq})$, where k is gas transfer velocity, C_w is concentration in the water, and C_{eq} is concentration in the water at equilibrium with the atmosphere. In the SRM, $k_{600} = c_1\,(\varepsilon{\cdot}\nu)^{1/4}{\cdot}Sc^{-n}$ where k_{600} is the gas transfer coefficient normalized to CO_2 at 20 °C, ε is rate of dissipation of turbulent kinetic energy, ν is kinematic viscosity, Sc is the Schmidt number, n is −1/2 with variability dependent on extent of surface films (Katul et al., 2018) but see Ho et al. (2018), and coefficient c_1 is ~0.5 (Katul et al., 2018; Lamont & Scott, 1970; Zappa et al., 2007) (See SI S.1.10). Rates of dissipation of turbulent kinetic energy can be obtained by direct measurements (Gålfalk et al., 2013; MacIntyre et al., 2018; Tedford et al., 2014). The magnitude of turbulence can be predicted within the framework of Monin-Obuhov similarity scaling (Monin & Obukhov, 1954) including newly developed equations for lakes (Tedford et al., 2014). In

the absence of wind, turbulence will be driven by convection (MacIntyre et al., 2018; Schladow et al., 2002). However, with light winds, wind-driven shear will dominate turbulence production at the air-water interface with the contribution of wind moderated by the extent of heating (buoyancy flux $\beta > 0$) and cooling ($\beta < 0$). Similarity scaling has been verified in a small pond (MacIntyre et al., 2018), and results using eddy covariance illustrate the accuracy of the similarity scaling for computing emissions and challenges when using eddy covariance at low wind speeds (Czikowsky et al., 2018). For improved understanding in flooded forests, predictions of ε from similarity scaling for $\beta < 0$ and $\beta > 0$ require validation with direct measurements of turbulence and calculations of k from the SRM require comparisons with those obtained using chambers.

Meteorology, thermal structure, and turbulence within tropical flooded forests have not been characterized, to our knowledge. Hence, we designed a study to quantify the physical drivers of gas exchange in flooded forests and to calculate k based on the SRM. We instrumented two flooded forests and adjacent lakes in the Amazon basin with thermistor arrays and meteorological stations, conducted chamber experiments of gas exchange, and measured turbulence with an acoustic Doppler velocimeter at one site. Our goal was to determine whether local cooling energized turbulence at night and the extent to which wind-induced flow in neighboring water bodies caused flows in the flooded forest that moderated near-surface turbulence. Understanding these physical mechanisms allows calculation of k and, in combination with measurements of gas concentrations, estimation of fluxes of carbon dioxide and methane within the extensive flooded forests of the Amazon (Melack, 2016; Melack & Hess, 2010).

2. Materials and Methods

The study was conducted in flooded forests of the Janauacá floodplain along the Solimões River and in the Anavilhanas archipelago in the lower Negro River. In Janauacá, the site was within a narrow bay near a larger open water area (Figure S1 in the supporting information (SI); 3.405722°S; 60.246889°W). Measurements were obtained from 28 August to 1 September 2016 (days 241 to 245). The flooded forest site in the Anavilhanas (Figure S1; 2.714343°S; 60.755320°W) was ~100-m east of the edge of Lake Prato (4.2 km^2 in area), and the open water site was ~50 from the edge of the flooded forest (2.7137°S; 60.75422°W). Measurements were made between midday 15 July and midday 18 July 2018 (days 196.5 to 199.5; Tables S1 and S2).

Temperature was measured using RBRsolo thermistors (0.002 °C accuracy) sampling at 2 Hz in Janauacá and 0.1 Hz in the Anavilhanas. Meteorological sensors were deployed ~2-m above the water on floating platforms in open water adjacent to the flooded forest in Janauacá and the Anavilhanas and inside the flooded forest of the Anavilhanas. A three-cup anemometer and wind direction sensor, shielded temperature and relative humidity sensors, and rainfall and photosynthetically available radiation (PAR) sensors were used. At Janauacá, incoming long and short-wave radiation was measured in the open with Kipp and Zonen CGR3 and CMP3 sensors. Outgoing long wave radiation was computed from surface water temperature. In the Anavilhanas, PAR was measured in the flooded forest with a photosynthetic irradiance logger. Vertical profiles of PAR were obtained with a Licor LI-192 SB sensor. See SI for more details.

An acoustic Doppler velocimeter (ADV, Nortek Vector) was deployed in the flooded forest in Janauacá. The depth of the measurement volume, l_v, was set to be 0.15-m below the water surface (see SI). Turbulence, as ε, was computed by fitting to the Nasmyth spectrum with quality controls verifying that Taylor's hypothesis was met and the turbulence isotropic (MacIntyre et al., 2018). Because turbulence is a lognormal process, data were arithmetically averaged (ε_{ma}). We verified that turbulence was occurring during periods when Taylor's hypothesis was not met by showing the persistence of root mean square vertical velocity fluctuations, w_{rms}, and obtaining values of buoyancy flux as $\beta_z = {w_{rms}}^3\, l$, where l is a mixing length, similar to estimates of buoyancy flux as calculated below and measured ε (see SI).

The surface energy budget, buoyancy flux β_o, and water friction velocity u_{*w} were calculated following Imberger (1985) and MacIntyre et al. (2002, 2014). Heat flux per unit area for 5-min intervals was computed from the surface energy budget (Q_M, J/m^2) and from time series of water temperature (Q_T, J/m^2; see SI).

We computed ε from the similarity scaling as $\varepsilon_s\ (\beta > 0) = (0.6 \cdot {u_{*w}}^3)/(\kappa \cdot z)$ and $\varepsilon_s\ (\beta < 0) = 0.77 \cdot |\beta| + 0.56 \cdot [{u_{*w}}^3/(\kappa \cdot z)]$, where $\kappa = 0.41$ is von Karman constant, $z = 0.15$ m, and positive β indicates heating

(Tedford et al., 2014). Buoyancy flux under cooling was also calculated from time series temperatures as $\beta_T = (g{\cdot}\alpha{\cdot}d\mathrm{T})/(dt{\cdot}l)$ where g is gravity, α is the coefficient of thermal expansion, $d\mathrm{T}/dt$ is the rate of change of temperature with time, and l is the vertical extent of thermals (see SI). k was calculated using the SRM as $k = [0.5{\cdot}(\varepsilon{\cdot}\nu)^{1/4}{\cdot}Sc^{-1/2}]$; ε was either measured with the ADV or computed as above (see SI). Values of k were normalized to CO_2 at 20 °C, k_{600}, using $Sc = 600$.

Fluxes (F) were obtained using floating chambers (Amaral et al., 2018; Barbosa et al., 2016), and k computed using $k = F/(C_w - C_{eq})$. When CO_2 in the chambers was measured with a SenseAir sensor (Bastviken et al., 2015), fluxes were computed for the initial linear output. CO_2 concentrations on both sides of the air-water interface were measured using an off-axis integrated cavity output spectrometer (Los Gatos Research Ultra-Portable Gas Analyzer) connected to a marble-type equilibrator for in-water values or with direct samples of air. Also, gas samples were obtained from water samples using the headspace method by vigorous shaking of equal volumes (30 ml) of water and air in the sampling syringe (Hamilton et al., 1995). Gas samples were injected into exetainers and measured within 3 months of collection with an infrared gas analyzer.

3. Results

3.1. Meteorology, Heat Fluxes, and Thermal Stratification

Conditions within the flooded forests were not conductive to wind-induced near-surface turbulence (Figures 1 and 2). Wind speeds were low within the protected embayment at Janauacá and in the channel in the Anavilhanas, rarely exceeding 2 m/s, and lower to negligible within the forests. Under low winds, for example 0.2 m s^{-1} with gusts to 0.5 m s^{-1}, sensible and latent heat fluxes ranged from −30 to −80 W/m^2 despite an unstable atmosphere induced by surface water temperatures warmer than air temperatures. Net long wave radiation (LWnet), which ranged from −75 to −110 W/m^2 in the open, consistently contributed to heat loss. Within the flooded forests, shading from the canopy reduced incoming solar radiation (Figures 2 and S2) but its influence on LWnet is uncertain. Effective heat flux, H_{eff}, exceeded 200 W/m^2 in open water and was less than 100 W/m^2 and sometimes negative in the flooded forests in the day (Figures 1 and 2). With high diffuse attenuation coefficients, 1.7 m^{-1} at Janauacá and 3 m^{-1} in the Anavilhanas, heat was trapped near the surface creating diurnal thermoclines in which the buoyancy frequency, N, reached 60 cycles per hour (cph) in Janauacá and 100 cph in the Anavilhanas (Figures 3, 4, S4, and S5). When cloud cover was sufficient, intervals of cooling occurred during the day. Heat was lost from late afternoon until early morning such that it was the dominant driver of turbulence throughout much of the day (Figures 1–4).

While wind did not directly induce shear near the water surface in the flooded forests, it indirectly induced flow if wind speed outside the forest exceeded 1 m/s. In the Anavilhanas, incoming and outgoing flows are indicated when Q_T, the change in heat content in the water, differed from Q_M computed from the surface energy budget. The difference is larger for westerly winds; the two terms were nearly in balance at night when winds were negligible outside the forest (Figures 2 and S5; see Texts S2.1 and S2.3). In Janauacá, measured flow speeds in the flooded forest increased from background flows <0.004 to 0.02 m/s when winds outside the forest were light (Figures 1; see Text S2.2). The flows were in opposition to the wind direction indicating they were alongshore, return flows driven by flow reversals relative to flows in open waters, an inference supported by three-dimensional hydrodynamic modeling (not shown).

3.2. Measured and Modeled Dissipation Rates, Buoyancy Flux, and *k* in Janauacá

Measured values of ε when $\beta < 0$ ranged from 2×10^{-9} to 2×10^{-7} m^2/s^3 (Figure 3a). ε_{ma} was ~3×10^{-8} m^2/s^3 for days 242–243 and days 244–245 and up to 1×10^{-7} m^2/s^3 for days 243–244. ε_{ma} was slightly lower than the predicted value of ε from the similarity scaling, ε_s, with the difference within the uncertainty of net long wave radiation within the flooded forest. β_T was nearly equal to ε_{ma}. The similarity of ε_{ma} to ε_s and β_T indicate cooling, as opposed to near-surface shear, was the primary driver of turbulence when $\beta < 0$ on days 242–243 and 244–245. An exception occurred before midnight on day 243 and early on day 244 when ε_{ma} was ~two times higher than β_T. At that time, near-surface flows were higher (Figure 1), and Taylor's hypothesis was more frequently met (Figure 3). The overall agreement between measured ε_{ma} and ε_s points to the accuracy in predicting near-surface ε when $\beta < 0$ from computed heat loss.

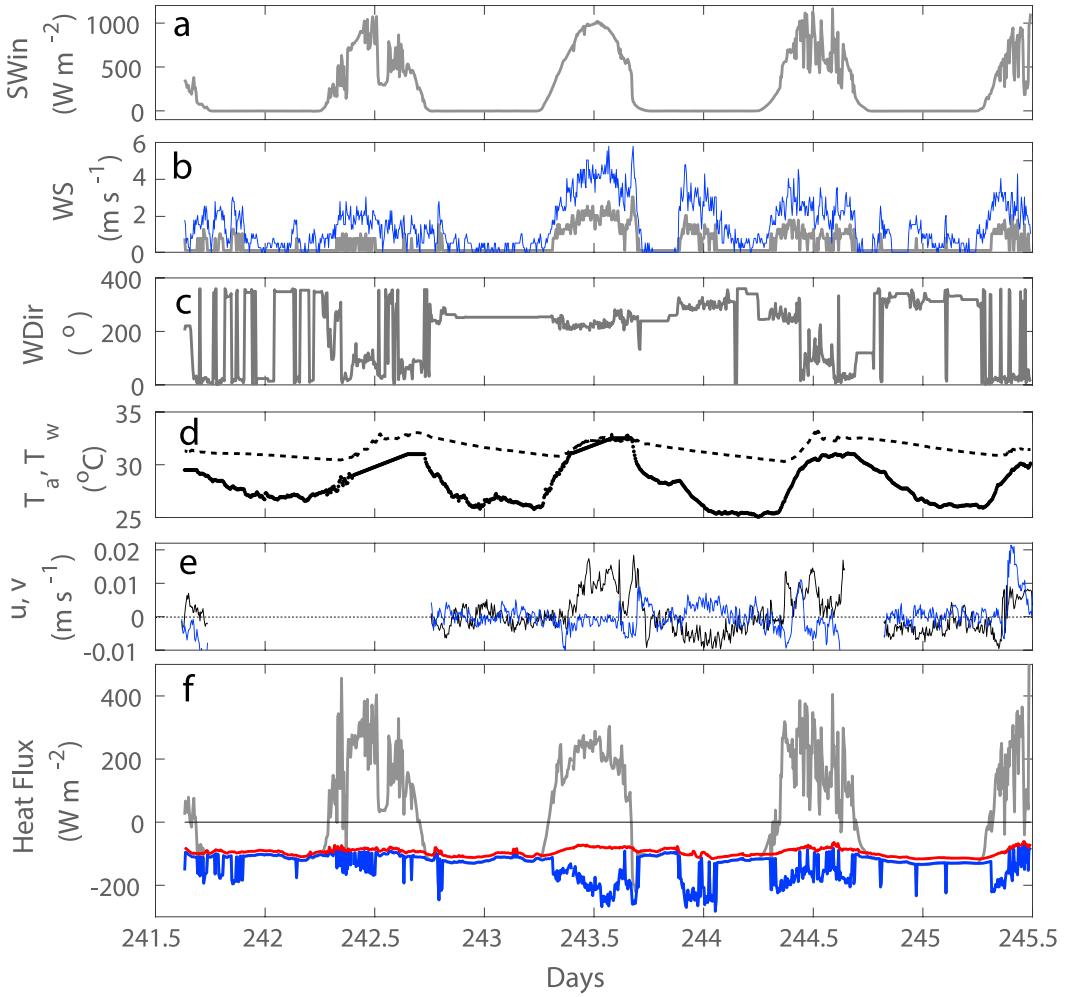

Figure 1. L. Janauacá. The 5-min averaged (a) incoming shortwave radiation (SWin), (b) mean WS (gray) and maximum WS (blue), (c) wind direction (WDir), (d) air temperature (T_a, black) and surface water temperature (T_w, dashed black), (e) horizontal currents speeds measured by the ADV (u, positive north; black; v, positive east, blue), and (f) heat fluxes with net long wave (red), surface heat flux (blue), and effective heat flux (gray). Gray indicates measurement was in embayment near flooded forest, black in the flooded forest, with effective heat flux computed from the composite data. WS = wind speed.

Measured ε declined with morning heating to values $\leq 10^{-8}$ m^2/s^3 (Figures 3a, 3c, and 3d). On mornings when winds were light in adjacent embayments, buoyancy frequencies N exceeded 25 cph, the maximum value at which the similarity scaling was found to hold (MacIntyre et al., 2018). However, with light winds and intermittent cloud cover on the morning of day 245, heat was mixed downward, $N < 25$ cph, and near-surface currents reached 0.02 m/s. Dissipation rates were elevated while the currents persisted and decreased when velocities declined. Each afternoon as the winds dropped and the diurnal thermocline downwelled prior to the onset of cooling, ε increased to values of ~10^{-7} m^2/s^3. The downwelling of the diurnal thermocline weakened the stratification such that $N < 25$ cph. The high ε on day 243.5 occurred when wind outside the forest gusted to 6 m/s. With strong stratification, turbulence at measurement depth was primarily anisotropic such that few valid measurements of ε were obtained. Once $N < 25$ cph, ε had values similar to predictions from the similarity scaling for light winds.

Values of k_{600} computed from the measured ε using the SRM were variable between 5-min periods, as expected for a process driven by turbulence (Figure 3b). Under cooling, estimated k_{600} varied from 1 to 4 cm/hr, and the arithmetic mean ranged from 3 to 4 cm/hr, similar or slightly lower than k_{600} predicted from the similarity scaling. Under heating, values ranged from 1 to 5 cm/hr. The low values occurred when the

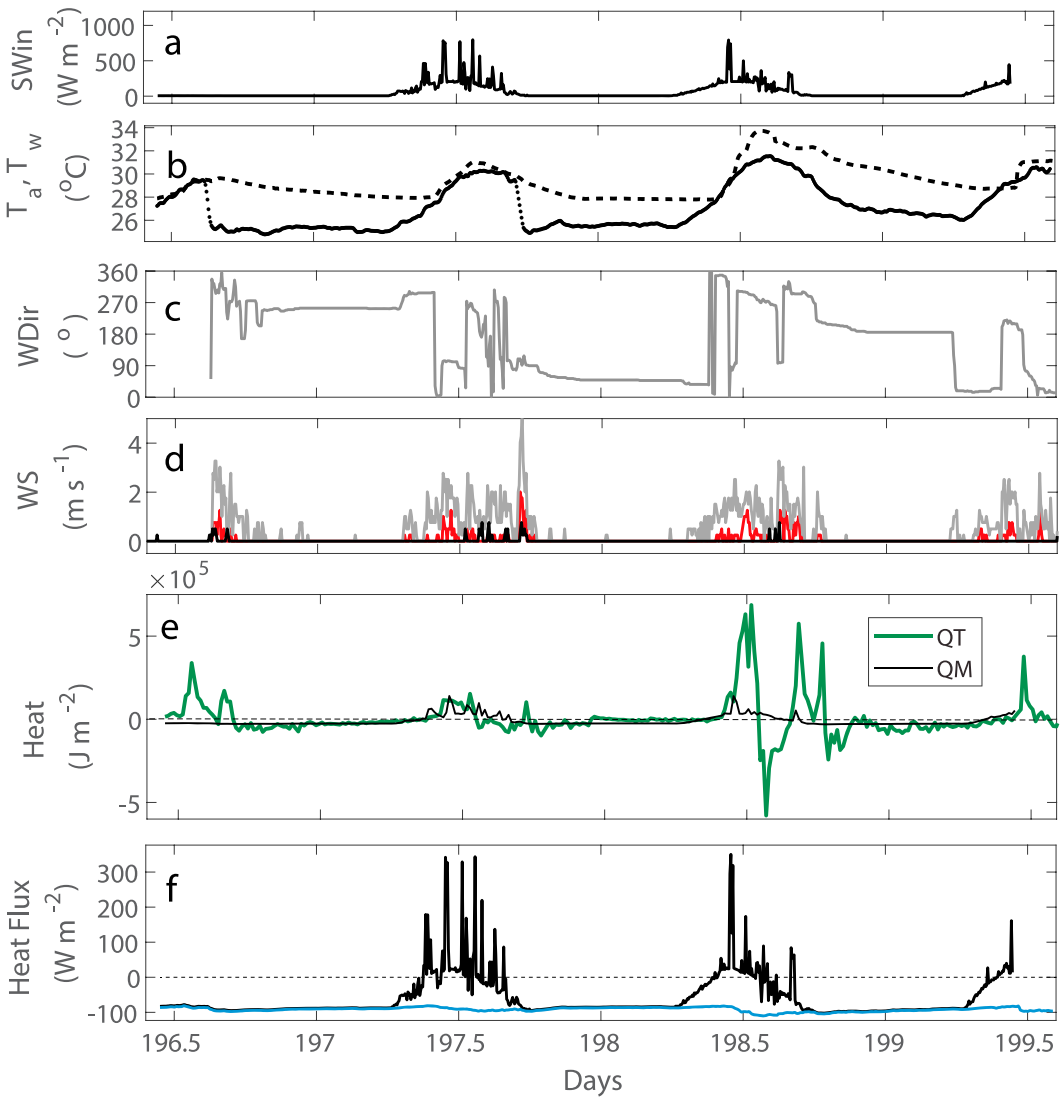

Figure 2. Anavilhanas. The 5-min averaged (a) incoming shortwave radiation (SWin), and (b) air temperature (T_a, black) and surface water temperature (T_w, dashed black) in the flooded forest; (c) wind direction (WDir), (d) maximum WS (gray) and mean wind speed (red) in the channel, and wind speed in the flooded forest (black), (e) 15-min smoothed time series of heat flux per unit area at 5-min intervals computed from the surface energy budget (Q_M, black) and from temperature in the upper meter in the flooded forest (Q_T, green), and (f) effective heat flux (black) and surface heat fluxes (blue) in the flooded forest. WS = wind speed.

water column became strongly stratified during morning heating, and higher values occurred as the diurnal thermocline downwelled. Values of k_{600} from the chamber measurements reflected the variability in the turbulence and were similar to predicted k_{600}. Values under cooling ranged from 1 to 4 cm/hr. Under heating, k_{600} ranged from negligible in the absence of wind to 5 cm/hr following wind gusts outside the forest of 3.5 m/s. The increased wind just after noon on day 244 induced a second vertical mode internal wave in the upper 0.3 m of the embayment and a similar one in the flooded forest. Such events will cause localized increases in flow speeds. In this case, northwesterly flow abruptly increased to 0.015 m/s, and N dropped below 15 cph.

3.3. Buoyancy Flux, Dissipation Rates, and Measured and Modeled *k* in the Anavilhanas

Dissipation rates computed from the similarity scaling had values at night of 5×10^{-8} m^2/s^3 (Figure 4a). When H_{eff} was positive in the day, ε_s could not be computed given the absence of wind. When the sign of H_{eff} was negative in the day, due to increased cloud cover combined with canopy shading, ε_s was also

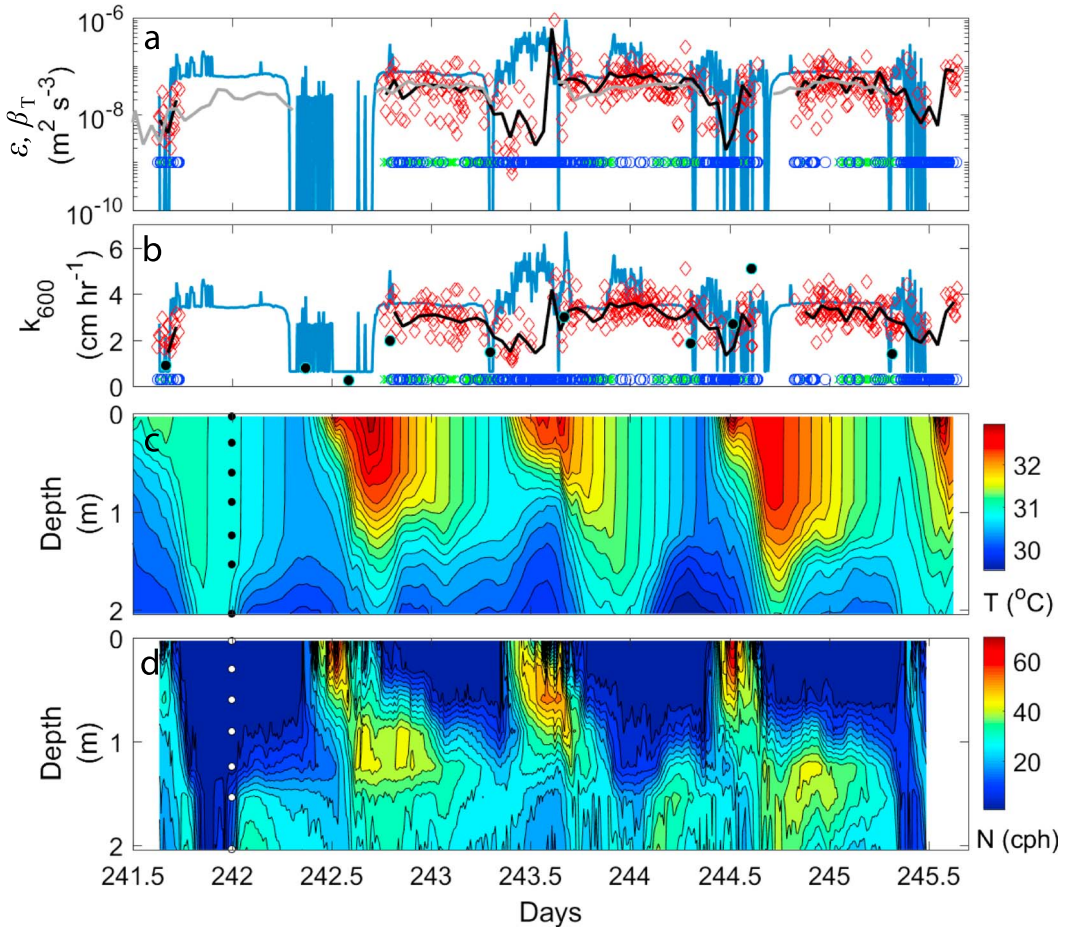

Figure 3. Flooded forest in L. Janauacá. Time series of (a) ε as measured by the acoustic Doppler velocimeter in the flooded forest (red diamonds), times when Taylor's hypothesis was not met (green x's), times when the turbulence was anisotropic (blue circles), running average of ε over 12 5-min averages of the measured data (ε_{ma} in the text; black line; intervals not meeting quality control were NaN'd), ε computed from ${u_{*w}}^3$ and β using the similarity scaling (blue, ε_s in the text), and buoyancy flux β_T computed from near-surface temperature change over time (gray line). β_T has not been multiplied by 0.8 as in the similarity scaling. (b) k_{600} computed from measured and computed ε with symbols and lines as in (a) and k_{600} obtained from chamber measurements (black circles), (c) temperature contours with half-hour averaging (black dots indicate sensor depths), and (d) buoyancy frequency (N) in cycles per hour, cph, as 10-min averages. Sampling rate of the acoustic Doppler velocimeter on initial run was 16 Hz and 8 Hz on the other two runs.

~10^{-8} m^2/s^3. β_T was ~10^{-8} m^2/s^3 when afternoon cooling began but typically tapered in the night as the rate of cooling decreased. Values of k_{600} computed using the SRM with ε_s obtained from the surface energy budget were zero during heating in the absence of wind, 2 cm/hr during heating with intermittent periods of cooling, and 3 cm/hr under steady cooling. The range is similar when computed from β_T although values would decrease as cooling tapered after midnight.

Values of k_{600} obtained using chambers ranged from 1 to 3 cm/hr and, with one exception, were lower than predicted based on ε under cooling (Figure 4b). During the day with its frequent cooling events, the contribution from cooling could not be distinguished from that due to flow between open water and the flooded forest (Figures 2e, 4b, and S5). The time series of measured ε indicates that variability in turbulence and resulting k_{600} are to be expected in the near-surface over short time periods (Figure 3).

4. Discussion

While air in flooded forests is nearly still, water immediately below is in motion and turbulent. Under cooling, rates of dissipation of turbulent kinetic energy measured using acoustic Doppler velocimetry ranged

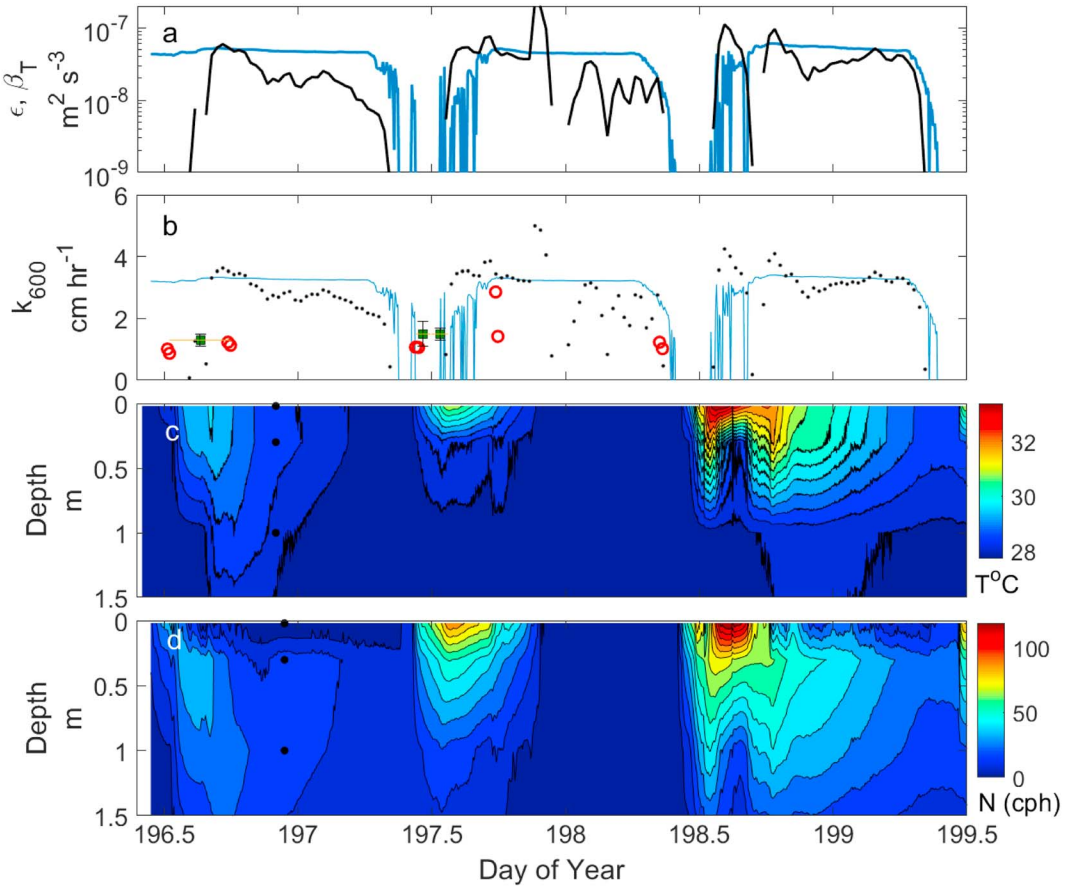

Figure 4. Anavilhanas flooded forest. Time series of (a) ε computed from the similarity scaling (blue) and β_T (black), (b) k_{600} computed from ε_s (blue line), β_T (black dots) and averaged k_{600} obtained from chamber measurements with the 10-min deployments (red) and 1.5- to 5-hr deployments (black, duration of deployment as horizontal bar and standard deviation as vertical bar), (c) water temperature in the upper 1.5 m, and (d) buoyancy frequency (N) in cycles per hour in the upper 1.5 m.

from 10^{-8} to 10^{-7} m^2/s^3. Dissipation rates were comparable to those observed in surface waters of lakes in the absence of wind and similar to those in a small pond with winds less than 2 m/s (MacIntyre et al., 2018; Tedford et al., 2014). Values such as these are considered moderate with lower values found either in highly stratified waters near the surface or deeper in the water column, similar values are found with breaking internal waves near lateral margins of lakes and under convection in larger water bodies, and higher values are found near the surface during windy conditions (Denman & Gargett, 1983; MacIntyre, 1993; MacIntyre et al., 1999). Under morning heating, values dropped below 10^{-8} m^2/s^3 but increased to 10^{-7} m^2/s^3 in the afternoon when winds increased outside the forest. At such times, horizontal flows increased up to 0.02 m/s inside the forest. Thus, wind acting on adjacent embayments increased near-surface turbulence in these sheltered locations.

With wind speeds at night below detection, turbulence was primarily driven by heat loss. This inference is supported by agreement with predictions based on buoyancy flux determined from surface meteorology and from temperature changes in the water. The cooling period minimally lasted from late afternoon until midmorning. Such a long duration has been observed in other tropical locations as warmer surface water temperatures increase heat losses (Augusto-Silva et al., 2018; MacIntyre et al., 2002) with canopy shading and cloud cover contributing here (Figures 2 and 4)

Internal waves with daily periodicity were prevalent in the flooded forests (Figures 3, 4, and S4–S6). Generated by winds outside the forest acting on the adjacent larger water body, they caused the diurnal thermocline to upwell or downwell depending on wind direction. Increased turbulence in the afternoon

occurred as the diurnal thermocline downwelled in Janauacá. Rather than near-surface shear being locally induced by wind, the shear that caused turbulence was induced by currents that flowed into the forest and induced internal waves. In the Anavilhanas, wind advected water into and out of the forest whereas in Janauacá, the flows were alongshore return currents.

Measured dissipation rates, ε_{ma}, agreed within a factor of 2 with values predicted by similarity scaling using local meteorology under conditions of weak stratification (Figure 3). Values of k_{600} calculated from chambers overlapped with the values computed using the SRM using ε from the ADV measurements (ε_{ma}) and similarity scaling (ε_s). This agreement shows that k_{600} can be computed from surface meteorology when stratification is weak in flooded forests. Measured ε and buoyancy flux predicted from hourly temperature change, β_T, were similar under cooling (Figure 3). This similarity implies that ε and k_{600} can be computed for other sites from temperature change when $\beta < 0$, as computed previously for shallow herbaceous wetlands (Ho et al., 2018; Poindexter et al., 2016; Poindexter & Variano, 2013). The lower measured values of ε during heating under calm conditions are to be expected as the depth of the measurement volume of the ADV was within the stratified diurnal thermocline rather than within an actively mixing layer.

Gas transfer velocities from floating chambers provide additional context when ε cannot be measured with the ADV, as with stronger stratification. During morning heating in the flooded forest when winds in adjacent open waters were low and intermittent and near-surface waters stratified, values of k_{600} obtained by chambers were sometimes negligible (~noon day 242, Janauacá) or ranged from 2 to 3 cm/hr (Figure 3). The variability in k_{600} reflected the variability in near-surface turbulence. The exchange of water in the flooded forest with that outside (Figures 1, 2, and S4–S6) also means that gases produced in the flooded forest could be exposed to conditions with higher near-surface turbulence which promote evasion. The combination of shear from wind-driven flows induced outside the forest and nocturnal cooling indicates that near-surface turbulence can be sustained in flooded forests. Consequently, k_{600} was typically of order 1 to 3 cm/hr, which when combined with CO_2 and CH_4 concentrations well above saturation (SI Text S2.4) and the extensive area of flooded forest, enables appreciable fluxes. The observations here as well as further experiments will enable improved assessment of fluxes from the extensive flooded forests which border the Amazon River and other tropical rivers.

Acknowledgments
Funding was provided by CNPq/MCTI n° 01300.001952/2018-66, U.S. Department of Energy contract DE-0010620, NASA grant NNX17AK49G, NSF DEB grant 1753856, and fellowships from CAPES and CNPq to J. H. F. A. and P. M. B. Lars Arneborg provided software for ADV processing. Two anonymous reviewers provided their helpful comments. Data are available at the National Center for Ecological Analysis and Synthesis Knowledge Network for Biocomplexity long-term archive (MacIntyre et al., 2019).

References

Amaral, J. H. F., Borges, A. V., Melack, J. M., Sarmento, H., Barbosa, P. M., Kasper, D., et al. (2018). Influence of plankton metabolism and mixing depth on CO_2 dynamics in an Amazon floodplain lake. *Science of the Total Environment*, *630*, 1381–1393. https://doi.org/10.1016/j.scitotenv.2018.02.331

Augusto-Silva, P. B., MacIntyre, S., de Moraesu, R. C., Cortés, A., & Melack, J. M. (2018). Stratification and mixing in large floodplain lakes along the lower Amazon River. *Journal of Great Lakes Research*, *45*(1), 61–72. https://doi.org/10.1016/j.jglr.2018.11.001

Barbosa, P. M., Melack, J. M., Farjalla, V. F., Amaral, J. H. F., Scofield, V., & Forsberg, B. R. (2016). Diffusive methane fluxes from Negro, Solimões and Madeira rivers and fringing lakes in the Amazon basin. *Limnology and Oceanography*, *61*(S1), S221–S237. https://doi.org/10.1002/lno.10358

Bastviken, D., Sundgren, I., Natchimuthu, S., Reyier, H., & Gålfalk, M. (2015). Technical Note: Cost-efficient approaches to measure carbon dioxide (CO_2) fluxes and concentrations in terrestrial and aquatic environments using mini loggers. *Biogeosciences*, *12*(12), 3849–3859. https://doi.org/10.5194/bg-12-3849-2015

Czikowsky, M. J., MacIntyre, S., Tedford, E. W., Vidal, J., & Miller, S. D. (2018). Effects of wind and buoyancy on carbon dioxide distribution and air-water flux of a stratified temperate lake. *Journal of Geophysical Research: Biogeosciences*, *123*(8), 2305–2322. https://doi.org/10.1029/2017JG004209

Denman, K. L., & Gargett, A. E. (1983). Time and space scales of vertical mixing and advection of phytoplankton in the upper ocean. *Limnology and Oceanography*, *28*(5), 801–815. https://doi.org/10.4319/lo.1983.28.5.0801

Gålfalk, M., Bastviken, D., Fredriksson, S., & Arneborg, L. (2013). Determination of the piston velocity for water-air interfaces using flux chambers, acoustic Doppler velocimetry, and IR imaging of the water surface. *Journal of Geophysical Research: Biogeosciences*, *118*, 770–782. https://doi.org/10.1002/jgrg.20064

Hamilton, S. K., Sippel, S. J., & Melack, J. M. (1995). Oxygen depletion and carbon dioxide and methane production in waters of the Pantanal wetland of Brazil. *Biogeochemistry*, *30*(2), 115–141. https://doi.org/10.1007/BF00002727

Ho, D. T., Engel, V. C., Ferrón, S., Hickman, B., Choi, J., & Harvey, J. W. (2018). On factors influencing air-water gas exchange in emergent wetlands. *Journal of Geophysical Research: Biogeosciences*, *123*(1), 178–192. https://doi.org/10.1002/2017JG004299

Imberger, J. (1985). The diurnal mixed layer. *Limnology and Oceanography*, *30*(4), 737–770. https://doi.org/10.4319/lo.1985.30.4.0737

Katul, G., Mammarella, I., Grönholm, T., & Vesala, T. (2018). A structure function model recovers the many formulations for air-water gas transfer velocity. *Water Resources Research*, *54*(9), 5905–5920. https://doi.org/10.1029/2018WR022731

Lamont, J. C., & Scott, D. S. (1970). Eddy cell model of mass transfer into the surface of a turbulent liquid. *Journal of the American Institute of Chemical Engineers*, *16*(4), 513–519. https://doi.org/10.1002/aic.690160403

MacIntyre, S. (1993). Vertical mixing in a shallow, eutrophic lake: Possible consequences for light climate of phytoplankton. *Limnology and Oceanography*, *38*(4), 798–817. https://doi.org/10.4319/lo.1993.38.4.0798

MacIntyre, S., Cortés, A., Amaral, J. H. F., Barbosa, P. M., Forsberg, B. R., & Melack, J. M. (2019). Meteorological, lake temperature, and dissipation rate time series in Amazon flooded forest, Brazil. *Knowledge Network for Biocomplexity*. https://doi.org/10.5063/F1HX1B0X

MacIntyre, S., Crowe, A. T., Cortés, A., & Arneborg, L. (2018). Turbulence in a small arctic pond. *Limnology and Oceanography*, *63*(6), 2337–2358. https://doi.org/10.1002/lno.10941

MacIntyre, S., Flynn, K. M., Jellison, R., & Romero, J. (1999). Boundary mixing and nutrient fluxes in Mono Lake, California. *Limnology and Oceanography*, *44*(3), 512–529. https://doi.org/10.4319/lo.1999.44.3.0512

MacIntyre, S., Jonsson, A., Jansson, M., Aberg, J., Turney, D. E., & Miller, S. D. (2010). Buoyancy flux, turbulence, and the gas transfer coefficient in a stratified lake. *Geophysical Research Letters*, *37*, L24604. https://doi.org/10.1029/2010GL044164

MacIntyre, S., Romero, J., & Kling, G. W. (2002). Spatial-temporal variability in surface layer deepening and lateral advection in an embayment of Lake Victoria, East Africa. *Limnology and Oceanography*, *47*(3), 656–671. https://doi.org/10.4319/lo.2002.47.3.0656

MacIntyre, S., Romero, J. R., Silsbe, G. M., & Emery, B. M. (2014). Stratification and horizontal exchange in Lake Victoria, East Africa. *Limnology and Oceanography*, *59*(6), 1805–1838. https://doi.org/10.4319/lo.2014.59.6.1805

Melack, J. M. (2016). Aquatic ecosystems In L. Nagy, P. Artaxo, & B. R. Forsberg (Eds.), *Interactions between biosphere, atmosphere, and human land use in the Amazon Basin: An introduction* (pp. 119–148). Berlin, Heidelberg: Springer Berlin Heidelberg. https://doi.org/10.1007/978-3-662-49902-3_7

Melack, J. M., & Hess, L. L. (2010). Remote sensing of the distribution and extent of wetlands in the Amazon Basin. In W. J. Junk, M. Piedade, F. Wittmann, J. Schöngart, & P. Parolin (Eds.), *Amazonian floodplain forests: Ecophysiology, ecology, biodiversity and sustainable management. Ecological Studies* (pp. 43–59). Dordrecht: Springer. https://doi.org/10.1007/978-90-481-8725-6_3

Monin, A. S., & Obukhov, A. M. (1954). Basic laws of turbulent mixing in the ground layer of the atmosphere. *Transactions Geophysics Institute Akademii Nauk USSR*, *24*(151), 163–187.

Monismith, S. G., Imberger, J., & Morison, M. L. (1990). Convective motions in the sidearm of a small reservoir. *Limnology and Oceanography*, *35*(8), 1676–1702. https://doi.org/10.4319/lo.1990.35.8.1676

Poindexter, C. M., Baldocchi, D. D., Matthes, J. H., Knox, S. H., & Variano, E. A. (2016). The contribution of an overlooked transport process to a wetland's methane emissions. *Geophysical Research Letters*, *43*, 6276–6284. https://doi.org/10.1002/2016GL068782

Poindexter, C. M., & Variano, E. A. (2013). Gas exchange in wetlands with emergent vegetation: The effects of wind and thermal convection at the air-water interface. *Journal of Geophysical Research: Biogeosciences*, *118*, 1297–1306. https://doi.org/10.1002/jgrg.20099

Schladow, S. G., Lee, M., Hürzeler, B. E., & Kelly, P. B. (2002). Oxygen transfer across the air-water interface by natural convection in lakes. *Limnology and Oceanography*, *47*(5), 1394–1404. https://doi.org/10.4319/lo.2002.47.5.1394

Tedford, E. W., MacIntyre, S., Miller, S. D., & Czikowsky, M. J. (2014). Similarity scaling of turbulence in a temperate lake during fall cooling. *Journal of Geophysical Research: Oceans*, *119*, 4689–4713. https://doi.org/10.1002/2014JC010135

Wang, B., Liao, Q., Fillingham, J. H., & Bootsma, H. A. (2015). On the coefficients of small eddy and surface divergence models for the air-water gas transfer velocity. *Journal of Geophysical Research: Oceans*, *120*, 2129–2146. https://doi.org/10.1002/2014JC010253

Zappa, C. J., McGillis, W. R., Raymond, P. A., Edson, J. B., Hintsa, E. J., Zemmelink, H. J., et al. (2007). Environmental turbulent mixing controls on air-water gas exchange in marine and aquatic systems. *Geophysical Research Letters*, *34*, L10601. https://doi.org/10.1029/2006GL028790